Impact of Pressure Profile on Contact Resistance using PGS in iPEBB Cooling

Joushua Padilla
Sea Grant Design Laboratory
Massachusetts Institute of Technology
Cambridge, MA
jgp07@mit.edu

Ethan Lietch
Sea Grant Design Laboratory
Massachusetts Institute of Technology
Cambridge, MA
ealietch@mit.edu

Julie Chalfant
Sea Grant Design Laboratory
Massachusetts Institute of Technology
Cambridge, MA
chalfant@mit.edu

Chryssostomos Chryssostomidis
Sea Grant Design Laboratory
Massachusetts Institute of Technology
Cambridge, MA
cmarge@mit.edu

***Abstract*— This paper presents the development of an experimental rig for testing thermal interface materials under various average pressures and pressure profiles. From the results of several experiments, an empirical model was developed that demonstrates the effect that interface pressure profile has on component temperatures when using Pyrolytic Graphite Sheets as the acting thermal interface material between the cooling solution and the heated system. The model uses the average interface pressure and the proximity of that pressure to the components as its independent variables. The model was then compared against temperature data collected under multiple random interface pressure profiles. This process can be extrapolated to the iPEBB system thus allowing the ESRDC to understand how critical structural design changes would affect the interface contact resistance between the iPEBB and the cabinet cold plate.**

Keywords—thermal management, power electronics, thermal interface material

I. Introduction

The Navy-funded Electric Ship Research and Development Consortium (ESRDC) works to advance technologies and concepts for electric ships. By electrifying ships, the Navy has the flexibility to control and direct energy where it is needed within a vessel [1]. One part of this effort is the development of the Navy integrated Power and Energy Corridor (NiPEC), which is a modular entity that encapsulates all the power handling requirements of a shipboard power and energy distribution system including transmission, conversion, protection, isolation, control and storage [2]. The basic component or least replaceable unit of the NiPEC is the Navy integrated Power Electronics Building Block (iPEBB) [9], which is envisioned to be a universal converter that is programmed for the specific application when installed [3]. iPEBBs may be combined in series or parallel to increase the voltage or current as required. The NiPEC will contain many, possibly hundreds of, iPEBBs. The iPEBB design is portable and replaceable, so the crew can easily swap out damaged or malfunctioning iPEBBs but leave the surrounding system in place if the equipment is still viable [2].

A sample iPEBB is shown in Fig. 1. The iPEBB is designed to be a rectangular shape and is depicted with outer substrate walls constraining the inner electrical components. This modular design allows the iPEBB to be easily ordered in expandable, compact grids within the power corridor of the ship [4].

One of the significant challenges involved in implementing an iPEBB-based power corridor is managing the thermal loads. A single iPEBB generates between 6 and 11 kW of waste heat and that heat must be removed in order to maintain the temperature of the internal components of the iPEBB below 150 C. Many solutions have been explored and considered. Air cooling solutions are limited in performance due to the low density, thermal conductivity, and specific heat of air. As heat loads increase, the amount of air or liquid required for cooling increases; in this example with 6kW of waste heat, the required pumping power for forced convection cooling, allowing a ten-degree Celsius temperature rise in the air, is 214W, whereas the pumping power for water as a heat transfer fluid with the same allowed temperature rise is only 0.35W [10]. Another factor that causes the air-cooling solution to be undesirable is the weight associated with adding a large aluminum heat sink to the top and bottom surfaces of the iPEBB. The iPEBB must remain under 16 kgs; therefore, installing heat sinks to the exterior of the iPEBB causes the weight of the iPEBB to exceed this limit. These reasons led to the further exploration of indirect liquid cooling.

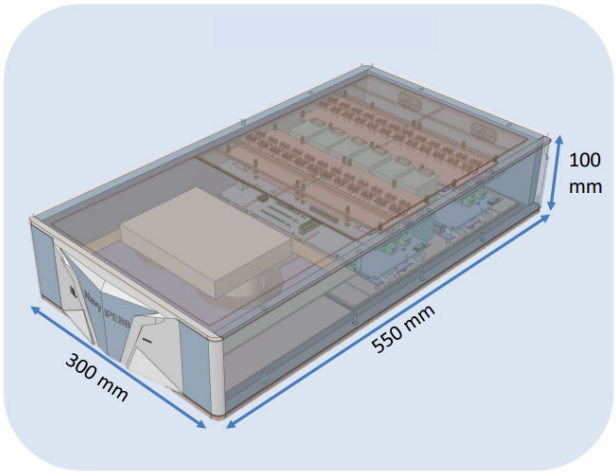

Fig. 1. The Navy iPEBB with dimensions annotated. Image courtesy of the Virginia Tech Center of Power and Energy Systems (CPES).

This material is based upon research supported by the U.S. Office of Naval Research (ONR) under award number ONR N00014-21-1-2124 Electric Ship Research and Development Consortium; and by the National Oceanic and Atmospheric Administration (NOAA) under Grant Number NA22OAR4170126-MIT Sea Grant College Program, and was approved for public release under DCN #543-359-23.

In the past couple of years, the ESRDC has pursued a cabinet cooling design concept that implements dry interface liquid cooling as the vehicle for thermal management of the iPEBB. The cabinet cooling concept was born out of the key design requirement that no liquid connections can be attached to the iPEBB itself because of its need to be modular and easily replaceable. This constraint causes the thermal management of the iPEBB to become more complex and challenging as direct component cooling is not possible.

Dry interface liquid cooling is accomplished via the use of a cold plate that is in series thermally with the iPEBB and that uses liquid convection to remove heat from the iPEBB. This concept evolved from the constraint that no liquid can enter the iPEBB structure itself. Thus, heat must be removed from the available outer surfaces of the iPEBB. The cold plate is incorporated into the cabinet system of the iPEBB stack. This presents the issue of contact resistance between the cold plate and the iPEBB, as the two cannot be permanently secured to one another.

A common way to lower contact resistance between two interfaces is through the use of a thermal interface material. Thermal interface materials (TIMs) are inserted between an electronic component that needs to be cooled and the cooling solution such as a heat sink in order to lower the contact resistance by filling in the small gaps between the surfaces when they are placed under a compressive load. This compressive load forces the thermal pad to fill the interstitial gaps between the components, supplying a conductive pathway where an air gap would have been. These interface materials vary in conductivity, Young's modulus, Poisson's ratio, as well as in the selected thickness.

The iPEBB application is somewhat different from the typical thermal interface application. Usually, thermal interface materials are used for a fairly small surface area, are applied in a clean environment in a factory, and are left in place for the lifetime of the equipment. The large interface area of the iPEBB application means that any significant required pressure for TIM performance will correspond to a very large required force on the installed iPEBB. There is also a challenge in providing even pressure across this full surface area. The plug-and-play nature of the iPEBB means that the TIM must be structurally robust so that it neither deteriorates with repeated installation nor leaves a fouled surface area in the cabinet where the replacement iPEBB will be installed. Since the TIM will be exposed to and installed in the shipboard environment, there is the possibility of the intrusion of grit in the interface surface. The TIM is intended to be pre-installed on the surface of the iPEBB, therefore must be lightweight to meet the weight constraints on the component.

One TIM material is the Pyrolytic Graphite Sheet (PGS). PGS was selected for further investigation due to its high in-plane conductivity, its light weight and structural integrity, and its usability compared to other Thermal Interface Materials. These qualities make it a high ranking candidate for the modular iPEBB system.

To determine the effectiveness and applicability of PGS as a thermal interface material between the iPEBB and the cold plate proposed in the dry interface liquid cooling design, experiments were conducted to determine how various pressure profiles affect the thermal behavior of the PGS and the impact on the heating elements of the iPEBB. The data collected from these experiments will be used to make recommendations on whether PGS should be used as a thermal interface material, and if so under what conditions for the best possible thermal performance, ensuring the chosen thermal management system can meet all of the thermal loads necessary.

II. Background

A. iPEBB

The iPEBB is designed to be easily transportable through narrow passageways and ladders within the ship, which leads to a necessary weight requirement of less than 16 kg. This is a significant restriction because the current weight of the iPEBB is 14.1 kg, thus severely limiting the scope of viable cooling options. To meet the weight requirement, the cooling system must be small and compact (under 1.9 kg); if this is not possible, the iPEBB would likely have to shed weight to meet its target value. A possible solution to the weight constraint is to focus the cooling mechanisms to the critical areas that generate heat.

The current Navy iPEBB is designed to be 300mm x 550mm x 100mm, as shown in Fig. 1. It is important to note that the dimensional requirements are not finalized, and the shape of the iPEBB could change in future iterations. Additionally, the iPEBB dimensions do not include any supplemental external parts needed by the cooling system. While the size of the cooling system is not mandated, the volume of the cooling mechanism contributes to the power density of the NiPEC and should therefore be minimized while remaining cost- and complexity-conscious.

The iPEBB is an enclosed box with electrical components that generate heat as they perform various processes to supply power to different operations within the ship. This is problematic because the heat generated within the box can only be transferred out into the environment through conduction, and a cooling mechanism is essential to increase the rate of heat transfer out of the system. If heat cannot be transferred out of the iPEBB efficiently, the operational power of the iPEBB must be decreased or components within the shell are at risk of damage. The cooling system must control the temperature of the most critical heat producing elements of the iPEBB: the MOSFET switches and the transformer, shown in Fig. 2. These elements produce essentially all the waste heat in the iPEBB and will subsequently have the highest temperatures within the iPEBB.

By imposing a rack-level cooling design on the top and bottom of the iPEBB, we can focus on cooling the critical concentrated heat loads generated by the rows of switches and the transformer. The MOSFET switches are depicted in the blue and red regions in Fig 2. It is important to note that the image in Fig 2 only displays the cross-sectional view of the top shell of the iPEBB, but there is a mirrored image on the bottom shell. This means that there is a total of four rows of switches within the iPEBB. Moreover, there is only one transformer located in the iPEBB. The top and bottom shell surfaces are denoted as the location for Rack Level Cooling; the cooling method will access these surfaces to remove heat produced by the MOSFET switches and the transformer [4].

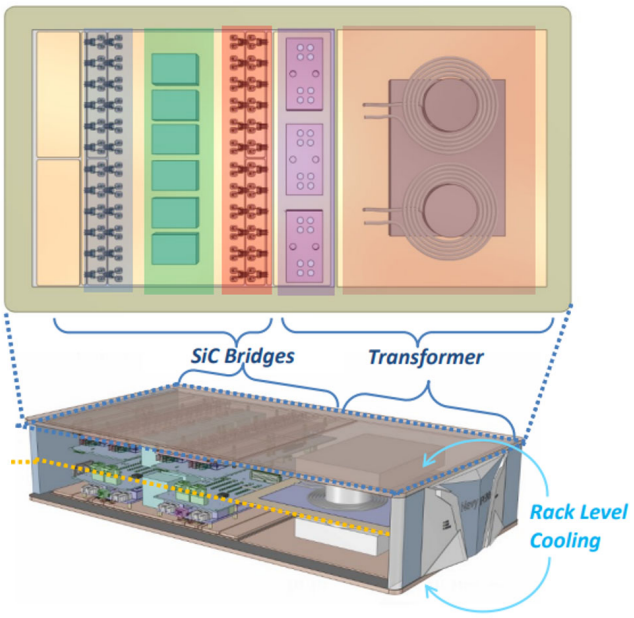

Fig. 2. The critical heat generation elements within the iPEBB are the MOSFET switches, depicted in the blue and red regions in the image. Image courtesy of the Virginia Tech Center of Power and Energy Systems (CPES).

1) SiC MOSFET Bridges

The critical heat-producing elements of the iPEBB are the SiC MOSFET bridges that are located inside the top and bottom shells. Both top and bottom substrates have two rows of switches consisting of 24 MOSFETs in each row, for a total of 48 switches per substrate and 96 switches in the entire iPEBB. The switches are in close proximity to one another which can lead to a significant heat concentration that will potentially deteriorate the electrical capability of the switches. As shown in the figure, the switches are spaced 2cm apart on center, which will lead to heat spreading effects between the switches [4].

The MOSFETs used in this application are approximated by a square prism shape with a thickness of 1mm and a side length of 0.8cm. Each MOSFET produces 100 W of waste heat, for a heat flux of 153 W/cm^2.

SiC MOSFETs generally have peak operational temperatures ranging between 150 to 200 C; thus, the current study will proceed with the goal of keeping each switch below 150 C. This is essential not only in the design for the extreme scenarios, but also because MOSFETs with lower operating temperatures are less expensive.

B. Thermal Interface Materials

Thermal Interface Materials (TIMs) are inserted between an electronic component that needs to be cooled and the cooling solution such as a heat sink in order to lower the contact resistance.

There are many different types of TIMs, ranging from the more standard and available silicon-based pads, to two-phase materials, to the material explored in this paper: graphite-based sheets. Each material has distinct advantages and disadvantages; thus, depending on the context of the system being examined and its design requirements, different TIMs will be better than others for a given application.

In this paper, the TIM that was explored in depth is the Pyrolytic Graphite Sheet (PGS). PGS is a synthetically produced material with a thin graphite film structure and high thermal conductivity. PGS is manufactured by heating a polymer film to its decomposition temperature in a vacuum. The film carbonizes then graphitizes, leaving a highly oriented graphite material. The graphene sheets are stacked on top of one another, promoting high in-plane thermal conductivity and thus heat spreading in the plane [5].

PGS is durable and can be reused many times without falling apart unlike many silicon-based or acrylic-based thermal interface materials. This quality makes it ideal for the modularity associated with the iPEBB stacks, so long as the PGS can meet the thermal constraints of the iPEBB and cooling system.

III. Experimental Design

A. Pressure Proximity Rig Design

To explore how pressure magnitude and profile affect the performance of the PGS on a heat load of shape similar to that of the iPEBB, a rig was designed such that two-dimensional pressure measurements and temperature measurements could be taken simultaneously without interfering with the thermal path between the resistor heated plate, which emulates the casing of the iPEBB, and the cold plate. To ensure no interruptions in the thermal path, the rig was symmetric about the midplane of the cold plate. This allows two identical interfaces to be created on either side of the cold plate: one for the pressure measurement and one for the heat transfer path. This symmetry allows the argument for pressure profile congruency between the two surfaces of the cold plate to be made, meaning that both interface pressure profiles and heating element temperatures could be recorded simultaneously. The pressure congruency argument does not take into account the differences in surface finish and manufacturing tolerances between the plates. This issue became more apparent when the repeatability of the rig's pressure and temperature performance were experimentally determined.

Specifically, the pressure proximity rig design, depicted in Figs. 3 and 4, contains four 1.5" x 1" resistors supplying heat to a 6" x 6" x 0.25" aluminum plate. The PGS is placed between this heated aluminum plate and the cold plate. This puts the PGS in the critical thermal interface between the first aluminum plate, which the resistors are attached to, and the cold plate, which supplies the cooling via chilled water to the system. The cold plate is the ATS-TCP-1021, which has 6 total passes of fluid through its stainless steel 0.5" ID piping. The dimensions of the ATS cold plate are 152mm x 119mm x 15mm with a total of 229 mm of piping for the coolant.

The pressure sensor is placed on the side of the cold plate furthest from the resistors. Atop the pressure sensor a second aluminum plate, identical to the first plate at the bottom of the stack, is added. Again, this places the pressure sensor at a position symmetric to the PGS about the midplane of the cold plate. This means that when a pressure load is applied, the PGS should experience the same pressure profile as the pressure

sensor allowing us to draw the pressure congruency arguments discussed earlier.

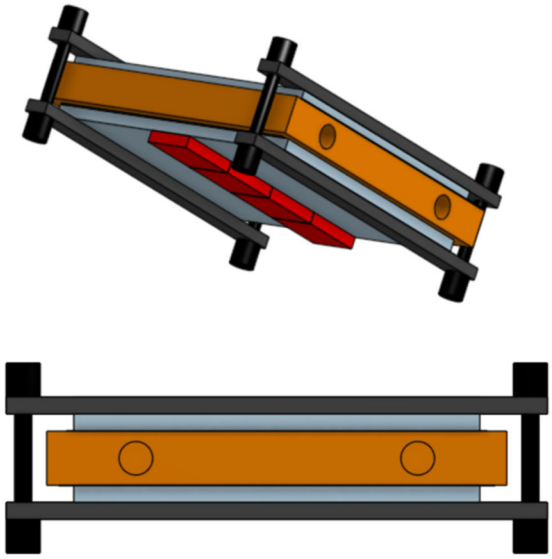

Fig. 3. CAD model of Pressure Proximity Rig

Pressure is applied to the stack via four 6-32 bolts. These bolts are passed through two sets of 12" x 0.5" x 0.5" steel braces, which ensure minimal bending deformation occurs in the aluminum plates; instead, the bending deformation is absorbed in the steel braces. The system contains ten total braces. Two each top and bottom on the far edges running parallel to the piping of the cold plate, and six running orthogonal to the original parallel supports, passing between the resistors. Due to the symmetry of the rig, the pressure experienced by the PGS is the same as the pressure experienced by the pressure sensor when the bolts are torqued.

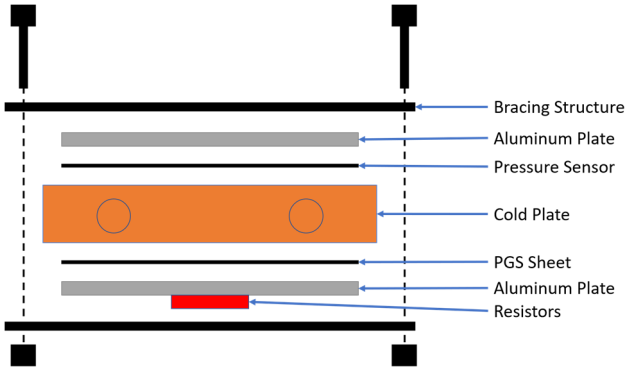

Fig. 4. Pressure Proximity Rig Exploded View

The full experimental rig can be seen in Fig. 5. The resistors are on the surface facing the camera, and the pressure sensor can be seen with green edges extending out to the left of the rig.

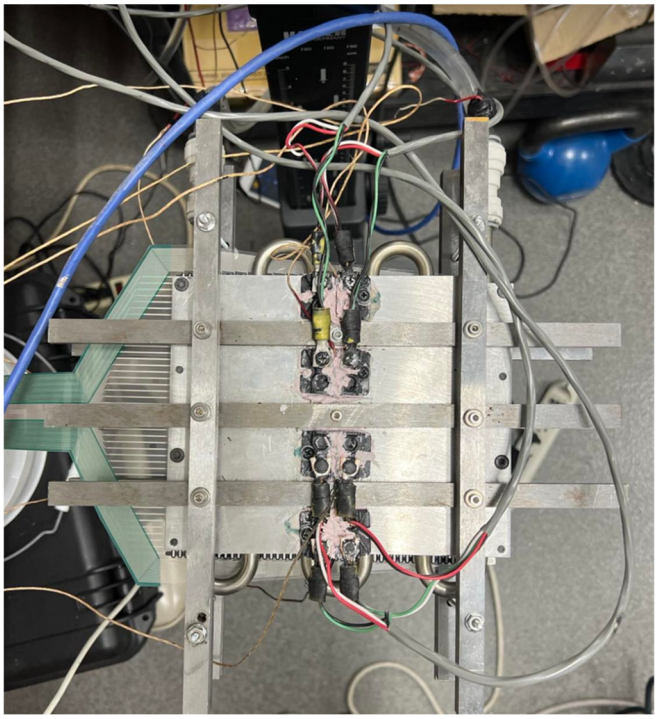

Fig. 5. Pressure Proximity Rig with cross bars and supports.

The results obtained by using this experimental setup are subject to both controllable and uncontrollable factors that may impact the data. The factors that are controllable include the pressure exerted on the system, the inlet temperature of the cooling water, the heating load of the heating elements, and the flow rate of the water. Factors that are not in the control of the setup include the ambient air temperature, the view factors associated with radiative heat transfer, and the manufacturing tolerances of the surfaces used in the pressure stack, specifically the top and bottom aluminum plates that are placed at the pressure and thermal interfaces and the faces of the cold plate. These factors must be considered and addressed when analyzing any data taken using the pressure proximity rig, and theoretical calculations and analytical models must be compared to the data to ensure some amount of congruency in the results.

B. Sensors

Within this rig, there were three types of sensors used: k-type thermocouples for sensing temperature, a Digiten flowrate sensor, and the Tekscan I-scan pressure mat. The associated ranges and uncertainties for these sensors are shown in Table 1. All sensors were calibrated before use.

The pressure senor that is used is the Tekscan I-scan 5151 pressure mat [8]. This mat has an array of 44 by 44 sensor elements, each approximately 1mm square. The pressure sensors are first equilibrated, then calibrated.

The sensors used in the experiments contained in this paper were taken to the Tekscan company headquarters in Massachusetts for equilibration. This process involves exerting a known uniform pressure on the sensor using specially designed rigs containing pressure bladders and compressed air, ensuring each of the cells report the same pressure. This

equilibration was accomplished at a set 10 PSI for the sensors used in the pressure proximity rig.

After the equilibration was completed, the calibration of the sensor was then conducted. The calibration was accomplished according to a multipoint calibration process discussed in depth in the I-scan manual [8]. The sensor was loaded with four different known masses. If the curve in the I-scan software between the measurements is confirmed to be linear, the process is successful and the calibration can be applied to any measurements conducted using the sensor. In the case of the sensors used in the data collected with the pressure proximity rig, the resulting calibration process was successful.

TABLE I. PRESSURE PROXIMITY RIG SENSORS AND PROPERTIES

Sensor	Manufacturer	Range	Uncertainty	Quantity
k-type thermocouples	Adafruit	-270 – 1372 C	2.2 C	7
Flowrate sensor	Digiten	1 – 30 LPM	Unknown	1
I-scan 5151 Pressure Mat	Tekscan	0 – 150 PSI	3% - 9%	1

IV. VERIFYING REPEATABILITY OF THE PRESSURE PROXIMITY RIG RESULTS

A. Profiles and Raw Pressure Data

Before conclusions can be drawn about the data taken using the pressure proximity rig, the repeatability of data produced by the rig must be established. The repeatability was determined by analyzing five different experiments with identical experimental settings. By holding the settings of the experiments constant, the repeatability of the rig could be determined by comparing the residuals of different pressure metrics and the resistor temperature data to the uncertainty associated with each of the sensors. The ambient conditions of the system were also recorded.

The uncertainty in measurements using the Tekscan pressure sensor is 3% – 9% of the average pressure recorded on the interface of interest [6]. For the k-type thermocouples used to measure the temperature of the four resistors on the rig, the associated uncertainty is 2.2 C [7].

To determine the repeatability of the pressure proximity rig results, five experiments were conducted under identical thermal and compressive loads. More specifically, the four screws that apply the pressure onto the PGS and the Tekscan pressure sensor were all tightened to the same torque of 4.0 in-lbs. An example of the pressure data maps/profiles recorded by the Tekscan pressure sensors is shown in Fig. 6.

The pressure data from these five experiments were compared via three different pressure metrics: average interface pressure, resistor pressure proximity value, and a cell-by-cell comparison.

The average interface pressure, P_{avg}, is simply the mean of all values recorded by the pressure sensor

$$P_{avg} = \sum_{i=1}^{k} [\frac{P_i}{k}] \quad (1)$$

where P_i is the pressure at the i^{th} cell on the pressure mat and k is the number of sensor elements, called sensels, in the pressure sensor being used. There are 1936 sensels arranged in a 44 by 44 grid in the sensor.

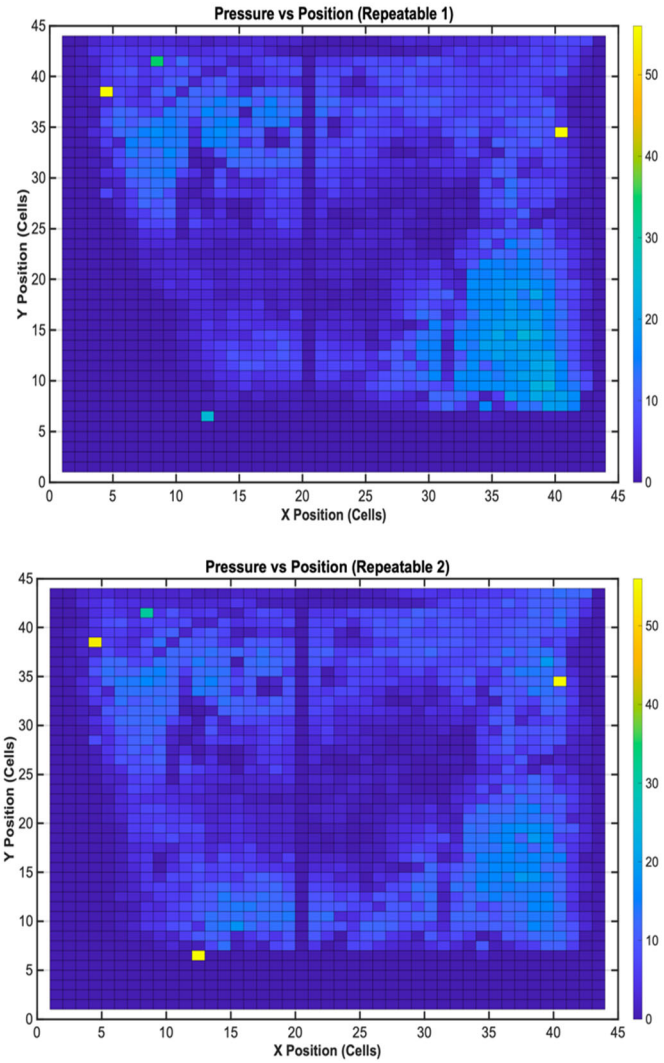

Fig. 6. Pressure profiles from two of the repeatability experiments with identical thermal and compressive loads.

The resistor proximity value, τ_n, was determined for each of the four resistors on the rig

$$\tau_n = \sum_{i=1}^{k} \frac{P_i}{d_{i,n} P_{avg}} \quad (2)$$

where $d_{i,n}$ is the distance to the i^{th} sensel from the n^{th} resistor and k is the number of sensels. The units of the proximity value, τ, are 1/distance due to the normalization by the average pressure of the interface. The proximity value of a given resistor is a measure of how much pressure is close to the resistor; a large value indicates pressure concentrated close to the resistor, and a small value indicates pressure concentrated away from the resistor.

The final pressure metric is the cell-by-cell measurement recorded by the pressure sensor, P_i. For the sake of these experiments, not every sensel was loaded. Thus, only the loaded sensels were used in the analysis. For the cell-by-cell comparison, these values were compared directly to one another across experiments. Thus, each sensel value was compared to the identical sensel from each of the experiments.

For the temperature metrics of repeatability, the values that were compared were the steady state temperatures of each of the four resistors on the rig. These steady state values were compared across the five experiments and thus allow for conclusions to be made regarding whether identical settings on the pressure rig result in the same resistor temperatures.

B. *Average Pressure Results*

As detailed above, the average pressure of the interface was determined using equation (1) for each cell located between the two plates. The average pressures and standard deviations for the five experiments can be seen in Fig. 7.

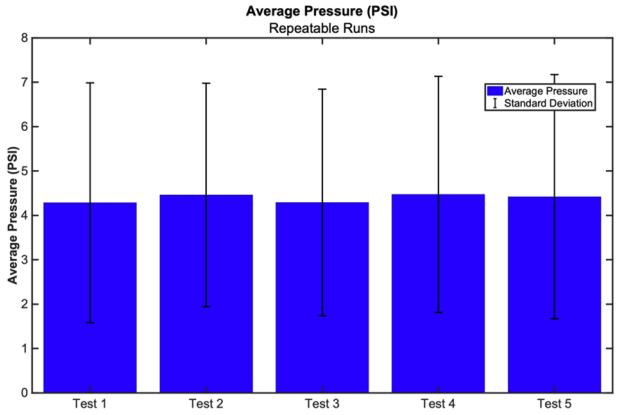

Fig. 7. Average pressure and standard deviations for five experiments to determine rig repeatability.

The mean average pressure across the five experiments, $\overline{P_{avg}}$, was 4.38 psi with a standard deviation of 0.0915 psi. The residual, R_P, of each experiment is

$$R_{P,m} = \frac{abs(P_{avg,m} - \overline{P_{avg}})}{\overline{P_{avg}}} \quad (3)$$

where m is the experiment number. The mean residual of the average pressure,

$$R_{P,avg} = \frac{1}{5}\sum_{i=1}^{5} \frac{abs(P_{avg,i} - \overline{P_{avg}})}{\overline{P_{avg}}} \quad (4)$$

can be compared the uncertainty of the pressure sensor. The calculated value using the five average pressures is $R_{P,avg} = 0.018$ or 1.8%. This residual value is less than the uncertainty associated with the pressure sensor when recording average pressure, whose range is 3-9%. Therefore, the pressure profile rig produces repeatable average pressures across the interface of interest, when all of the experimental settings are held constant.

C. *Proximity Value Data*

To examine the proximity value repeatability, a similar process was used. First, the proximity values for each resistor, in each experiment, were calculated using (2). Next, the means and standard deviations for the proximity value of each resistor across the five experiments were calculated. These results can be seen in Fig. 8.

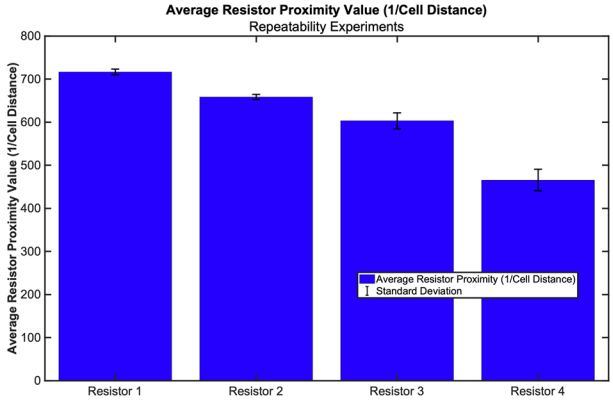

Fig. 8. Average proximity values for each of the four resistors across all five experiments.

The average proximity value residual value was determined using a process similar to the that used to calculate the residuals of the average pressure measurements. First, the average proximity values for each resistor were calculated across the five experiments. These values will be denoted as $\overline{\tau_{avg,n}}$, where n is the resistor for which the value is calculated. The proximity value residual $R_{\tau,n,m}$ for the n^{th} resistor in the m^{th} experiment is

$$R_{\tau,n,m} = \frac{abs(\tau_{avg,n,m} - \overline{\tau_{avg,n}})}{\overline{\tau_{avg,n}}} \quad (5)$$

Each of these 20 residual values were then averaged across the five experiments. This yielded a mean average proximity value residual of 0.0375, or 3.75%. The residual calculated is within the lower end of the uncertainty range of 3 – 9% for the sensor. Thus, the pressure proximity rig is able to repeatably produce resistor proximity values across the interface of interest, when all of the experimental settings are identical.

D. *Cell to Cell Data Across Experiments*

The last metric used to check the repeatability of the pressure profiles compares the exact profiles from each experiment to one another. This means each cell was compared to the identical cell across all five repeatability experiments. To determine an average profile, S_{avg}, the five profiles were averaged

$$S_{avg} = \frac{1}{m}\sum_{j=1}^{m} P_j \quad (6)$$

where m is the number of experiments. Thus, S_{avg} is a matrix of the same size as P. This average profile is then used to calculate the residuals of each cell for each of the five experiments, where

$$R_{S,avg} = \frac{1}{k}\sum_{i=1}^{k} \frac{abs(P_i - S_{avg,i})}{S_{avg,i}} \quad (7)$$

with a resultant value that indicates the average residual value of the k cells on the Tekscan pressure mat for each experiment.

These values are plotted in Fig. 9. The average residual across all five experiments is

$$\overline{R_{S,avg}} = 0.2727 \sim 27\% \quad (8)$$

which is much higher than the 9% maximum uncertainty value detailed above. Thus, the pressure proximity rig cannot produce repeatable pressure profiles on a cell-by-cell basis across the interface of interest, when all of the experimental settings are identical. This may be due to slight changes in the position of the pressure mat relative to the surface finish of the plates.

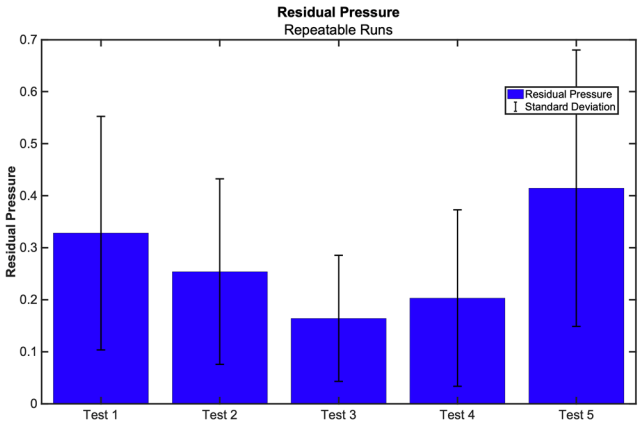

Fig. 9. Average profile residuals for each experiment.

These results and analysis indicate that the rig can produce repeatable profiles when characterized by average pressure and resistor proximity value, but cannot produce repeatable profiles on a cell-by-cell basis. As can be seen in the next section, cell-by-cell repeatability is not required to produce repeatable resistor temperature results.

E. Corresponding Temperature Data

Now that the pressure metrics have been worked through, the next step to determining the repeatability of the proximity pressure rig is to look at the temperature metrics. The temperature metrics used to determine this were the four steady-state resistor temperatures, the ambient air temperature, and the inlet water temperature. These temperatures were recorded using four k-type thermocouples with uncertainties of 2.2 degrees Celsius.

While assessing the four resistor temperature metrics it is important to keep in mind the assumption that the inlet water temperature to the cold plate and the ambient temperature (which can both be referred to as the fluid temperatures) were identical in the five tests for repeatability. The inlet and ambient temperatures were tracked using the same k-type thermocouples as the resistor temperatures. For the fluid temperatures to be determined as repeatable across experiments, the standard deviation of the five measurements for the ambient and inlet fluid temperatures must be smaller than the uncertainty of the sensor, 2.2 C. For the inlet water temperature, the mean and standard deviation across the five repeatability experiments were 29.4+/-0.2 C. For the ambient air temperature, the mean and standard deviation were 31.6+/-0.4 C. The standard deviations of these measurements were both smaller than the thermocouple uncertainty, meaning the data collected in the five repeatability experiments was collected under identical thermal conditions.

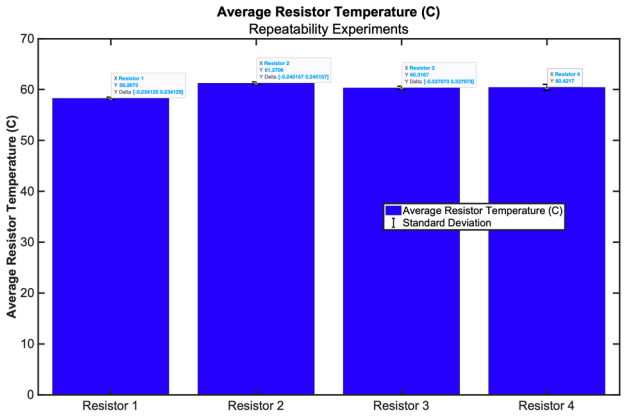

Fig. 10. Average steady state resistor temperatures across the five repeatability experiments.

To determine whether the resistor temperature results collected were repeatable, the data from each resistor across the five experiments was averaged on a resistor-by-resistor basis;

$$T_{avg,n} = \sum_{i=1}^{m} T_{n,i} \quad (9)$$

where n is the resistor number and m is the number of experiments; the results are plotted in Fig 10. The residuals for the temperature values are calculated as

$$R_{T,n,m} = abs(T_{actual,n,m} - T_{avg,n}) \quad (10)$$

These residuals are then averaged as an aggregate. The mean average residual resistor temperature is 0.5±0.3 C. This residual value is less than the uncertainty associated with the k-type thermocouples used for measurement. This means that, under identical experimental settings, the resistor temperatures are reproducible.

Consequently, from the five identical experiments conducted to determine the repeatability of the pressure proximity rig, it was determined that resistor temperature, resistor proximity value, and average interface pressure are reproducible, while the exact pressure profile, on a sensel-by-sensel basis, is not reproducible. Note that the resistor temperatures are well within the uncertainty bounds of the sensors. The fact that the temperature data is repeatable with residuals well within the uncertainty bounds of the sensors indicates that cell-to-cell repeatability in pressure measurements is not necessary to achieve repeatable results.

V. Pressure Proximity Rig Test Results

The goal of the pressure proximity rig is to create varied pressure profiles across the surface in a controlled manner, then quantify the impact of the varied profiles on the performance of the thermal interface material. Three sample pressure profiles can be seen in Fig. 11, in which the top image shows an even profile, the middle image shows pressure concentrated along the left side of the plate, and the bottom image shows pressure concentrated along the top edge of the plate.

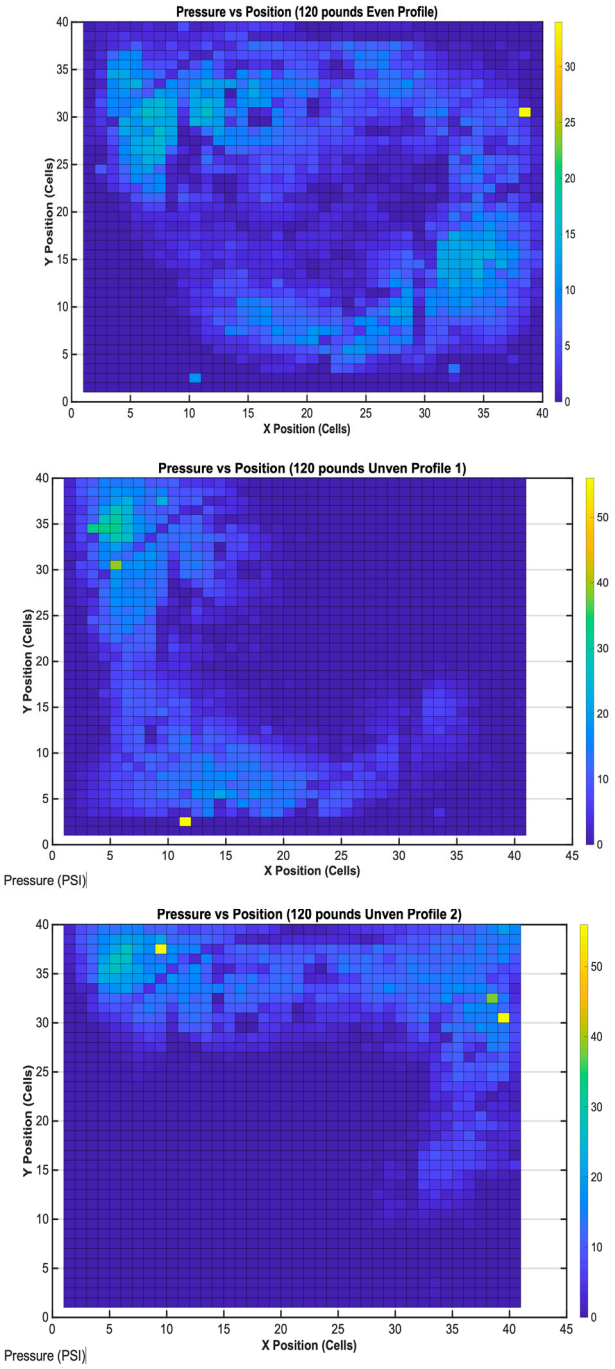

Fig. 11. Pressure profiles created using the pressure proximity rig showing even pressure across the full surface (top image), pressure concentrated along the left side of the rig (middle image), and pressure concentrated across the top of the rig (bottom image).

A set of experiments was run with a pre-planned arrangement of pressure profiles and overall average pressures. One example run is shown in Fig. 12. Resistors are numbered from right to left. It is evident from the pressure profile that pressure is concentrated on the left-hand side of the surface; thus, resistor R4 has a much higher pressure-proximity value than resistor R1. The resistor temperatures for this run display a clear inverse correlation between pressure proximity value and temperature, displayed in the plot at the bottom of Fig. 12.

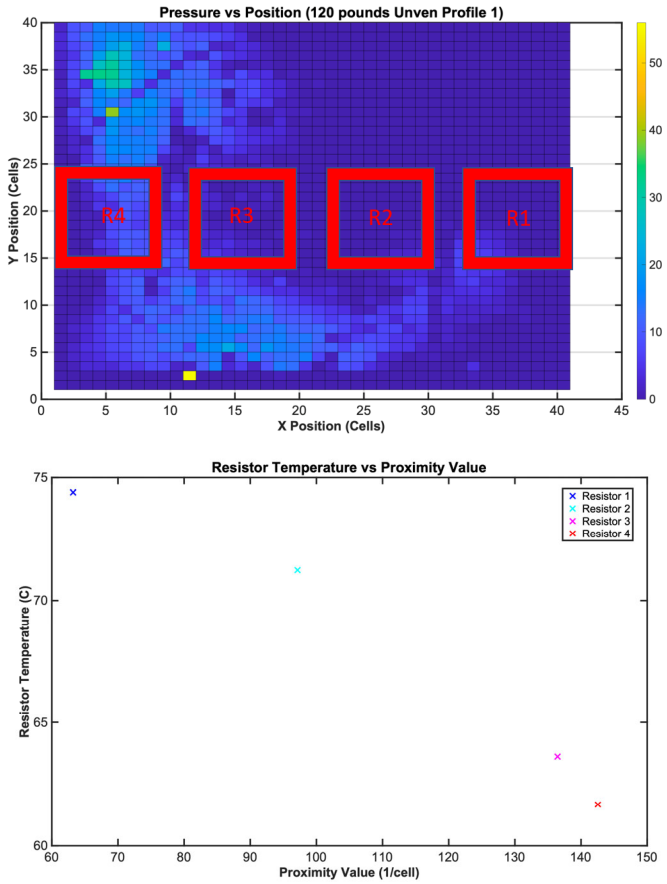

Fig. 12. Pressure profile and individual resistor temperatures for a single experiment, showing inverse correlation between pressure proximity value and temperature.

VI. Predictive Model for the Pressure Proximity Rig

A. Model Development

The next step in this research was to formulate an empirically derived predictive model for the resistor temperatures based on the controllable pressure metrics. The model will be a linear least squares model of the form

$$T_{n,predict} = C_0 + C_1 P_{avg} + C_2 \tau_n \qquad (11)$$

with two independent variables: interface average pressure, P_{avg}, and resistor proximity value, τ_n. The dependent variables in this case are the steady state temperatures of each of the four resistors on the rig. Thus, using the average pressure value and the resistor proximity value, the model should meaningfully predict the steady state temperature of any individual resistor.

The data used to develop this model was generated in eleven random experiments in which the average pressure and profile shapes were not specified but instead the rig's pressure creating screws were tightened to random torques creating random profile shapes. These 11 experiments were all conducted under

the same thermal settings such that ambient temperature, water temperature, water flowrate, etc., were consistent throughout. Using the Matlab integrated least squares solver produced the coefficients shown in (12).

$$T_{n,predict} = 77.4262 - 2.4404P_{avg} - 0.0379\,\tau_n \quad (12)$$

indicating a negative correlation between resistor temperature and the two independent variables, P_{avg}, and τ_n, which intuitively makes sense. The higher the average pressure, the lower the temperature should be. Likewise, the closer the pressure is to the resistor of interest, the lower the temperature of that resistor should be.

B. *Accuracy of the Model*

To gauge how good the model was in predicting resistor temperature from P_{avg}, and τ_n, 10 more experiments were conducted. These experiments were again in the same 0 – 6 PSI range. These 10 experiments supply 40 resistor temperature data points for comparison to the predictive model.

To make this comparison, first the data was collected and processed into, τ_n, P_{avg}, and $T_{n,actual}$. The pressure data, P_{avg} and τ_n, for each of the resistor data points (40 in this set of experiments), was then used in (12) to derive 40 resistor temperature predictions, $T_{n,predict}$. The predicted temperatures were then compared to the actual temperatures. Residuals were calculated in two ways: with a percentage comparison, $R_{\%}$ and a degree comparison, R_{deg}, where

$$R_{\%} = 100\frac{\sqrt{(T_{n,actual}-T_{n,predict})^2}}{T_{n,actual}} \quad (13)$$

and

$$R_{deg} = \sqrt{(T_{n,actual} - T_{n,predict})^2} \quad (14)$$

The result was 40 values for each of these residual calculations. The average residuals between the predictive model and the actual temperatures, with the same P_{avg}, and τ_n, are 2.5 C ± 2.0C for the degree comparison, and 3.7% ± 2.9% for the percentage comparison. This means that the predictive model can predict the resistor temperature on the pressure proximity rig within 2.5 C ± 2.0C, with only the average pressure on the thermal interface P_{avg}, and the proximity value for that resistor, τ_n.

To visualize the prediction space related to the actual temperature values from the 40 experiments, Fig. 13 shows these comparisons. Note that maximum error is less than 7 C. The predicted space is of all of the possible resistor temperatures from the ranges of P_{avg}, and τ_n, that are within the axis ranges.

The results of these experiments provide a thorough empirical analysis of how to predict heating element temperature from known pressure metrics of average interface pressure and proximity value.

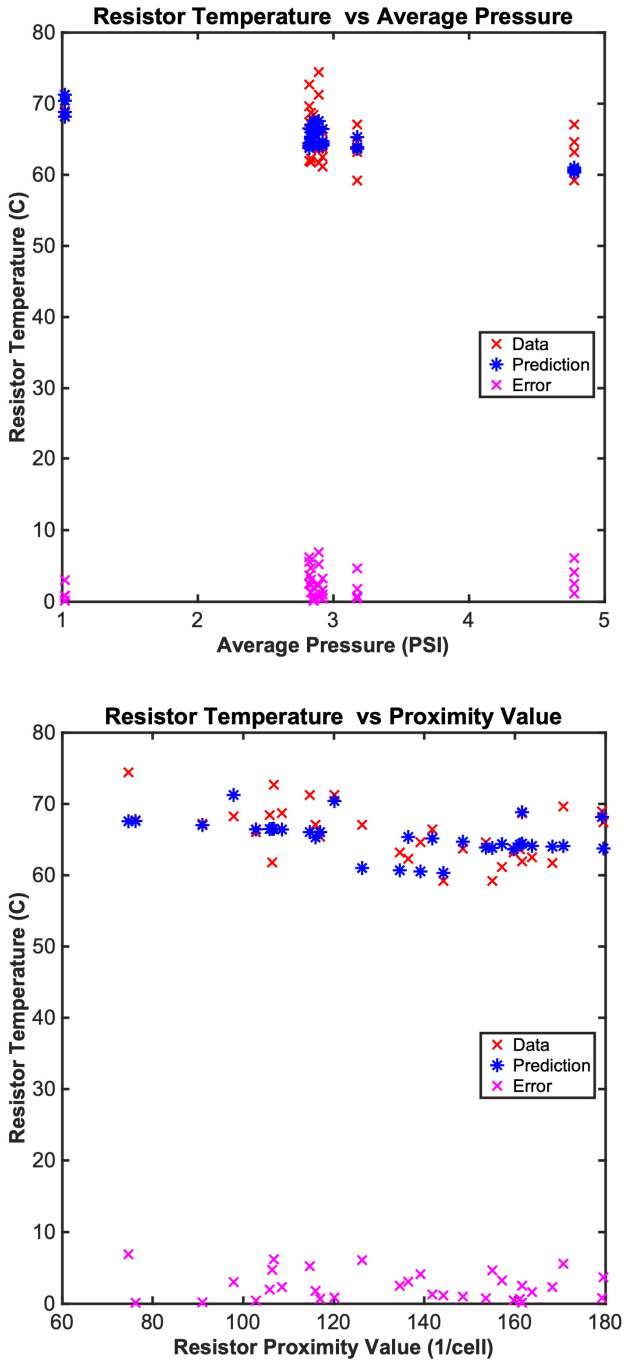

Fig. 13. Predicted and actual resistor temperatures plotted versus P_{avg} (top) and τ (bottom).

C. *Discussion*

The empirically derived linear least-squares model has an accuracy of 2.5 C ± 2.0C. This accuracy is quite high considering the uncertainty of the thermocouples used to collect the temperature data is 2.2 C. The derivation of this model, using the experimental design that leverages average pressure and proximity value as independent variables can be replicated on any flat system that might require a TIM paired with an interface pressure to ensure good heat transfer. What the results of the

model show is that pairing the Tekscan I-scan pressure sensor with thermocouples monitoring component steady state temperatures to produce a linear least squares model, produces a model that can predict component temperatures within 4% of the actual system thermal behavior.

From the predictive temperature model in equation 13, the coefficients associated with the two independent variables reveal what factors dominate component temperature. The magnitude of the constant associated with the average pressure of the interface is over 64 times larger than the magnitude of the constant associated with the proximity value. This simple analysis and comparison indicate how average interface pressure affects the final component temperature much more than the components proximity value on the pressure proximity rig.

The empirical model that was derived, and its presented accuracy, indicate how important understanding how pressure will be applied to the iPEBB cold plate interface. Understanding what this pressure profile will look and pairing this understanding with live thermal testing in a similar manner to what was conducted for the pressure proximity rig will give the ESRDC the data needed to be able to predict iPEBB thermal performance from interface pressure profiles.

VII. Conclusions and Future Work

This paper has presented the design and testing of an experimental rig for testing thermal interface materials under various average pressures and pressure profiles. From the results of several experiments, an empirical model was developed that demonstrates the effect that interface pressure profile has on component temperatures with PGS as the acting TIM between the cooling solution and the heated system. The empirical model's demonstrated accuracy of 3.7% when predicting component temperatures is very promising when considering the relatively low complexity of the model's inputs.

Moving forward, the accuracy of the predictive model is promising when thinking about the methods and processes used to create this model. The same methods used in this paper, on the pressure proximity rig, can be applied to the actual iPEBB to cold plate interface once system level designs of the iPEBB stack structure are farther along. Parallel work is ongoing to characterize the thermal conductivity of PGS under uniform thermal and compressive loads at low pressures. The information described in this paper coupled with the thermal conductivity characterization and the models under development will allow the ESRDC to make thermally informed decisions on the iPEBB cooling and clamping systems; understanding how structural design changes will affect the interface contact resistance between the iPEBB and the cabinet cold plate.

Acknowledgments

The authors express their appreciation for the collaboration with Dr. Christina DiMarino and Narayan Rajagopal of the Virginia Tech Center for Power and Energy Systems (CPES).

References

[1] "GE Powers US Navy's 1st Full-electric power and propulsion ship," *GE News*. [Online]. Available: https://www.ge.com/news/press-releases/ge-powers-us-navy%E2%80%99s-1st-full-electric-power-and-propulsion-ship. [Accessed: 26-Mar-2022].

[2] C. Cooke, C. Chryssostomidis, and J. Chalfant, "Modular integrated power corridor," in *Electric Ship Technologies Symposium (ESTS), 2017 IEEE*. IEEE, 2017, pp. 91–95.

[3] T.Ericsen, N.Hoingorani, and Y.Khersonsky,"PEBB–power electronics building blocks from concept to reality," in *IEEE Petroleum and Chemical Industry Technical Conference 2006 (PCIC06)*. IEEE, September 11-13, 2006, paper PCIC-2006-22.

[4] Rajagopal, N. (n.d.). Navy Integrated Power Electronics Building Block (Navy iPEBB). *Electric Ship Research and Development Consortium*.

[5] "Pyrolytic graphite," *Pyrolytic Graphite - Thermal Interface Material | HPMS Graphite*. [Online]. Available: https://hpmsgraphite.com/pyrolyticgraphitesheet?gclid=CjwKCAjwzeqVBhAoEiwAOrEmzRKAVonwnRXRTnOX4kR7lwJBfMpAkncuaX4MkVAwK6ueok-U812NyBoCrAwQAvD_BwE%29. [Accessed: 02-Mar-2023].

[6] K. Bachus, A. Demarco, K. Judd, D. Horwitz, D. Brodke. (2006). Measuring contact area, force, and pressure for bioengineering applications: Using Fuji Film and TekScan systems. *Medical Engineering & Physics*. 28. 483-488. 0.1016/j.medengphy.2005.07.022.

[7] "Thermocouple," *Thermocouple accuracies - Thermocouple Accuracy - Thermocouple Accuracy Comparison Chart*. [Online]. Available: https://www.thermocoupleinfo.com/thermocouple-accuracies.htm. [Accessed: 02-Mar-2023].

[8] Tekskan, Inc. *I-scan™ & High Speed I-scan User Manual.* South Boston, MA. 2018.

[9] N. Rajagopal, C. DiMarino, R. Burgos, I. Cvetkovic and M. Shawky, "Design of a High Density Integrated Power Electronics Building Block iPEBB Based on 1.7 kV SiC MOSFETs on a Common Substrate," *2021 IEEE Applied Power Electronics Conference and Exposition (APEC)* 2021 pp 1-8.

[10] J. Padilla, *Characterizing the Thermal Behavior of Pyrolytic Graphite Sheets (PGS) at Low Interface Pressures*. Master's thesis, Massachusetts Institute of Technology, 2023.